Stability of oxidized states of ceria-supported PtO_x particles under a wide range of gas-phase conditions

Jon Eunan Quinlivan Domínguez,[1] Konstantin Neyman,[1,2] Albert Bruix[1,*]

[1]*Departament de Ciència de Materials i Química Física and Institut de Química Teòrica i Computacional (IQTCUB), Universitat de Barcelona, 08028, Barcelona, Spain*

[2]*ICREA (Institució Catalana de Recerca i Estudis Avançats), 08010 Barcelona, Spain*

*corresponding author: abruix@ub.edu

ABSTRACT: Nanostructured materials based on non-inert oxides CeO_2 and Pt_yO_x play a fundamental role in catalyst design. However, their characterization is often challenging due to their structural complexity and the tendency of the materials to change under reaction conditions. In this work, we combine calculations based on the density functional theory, a machine-learning assisted global optimization method (GOFEE) and *ab initio* thermodynamics to characterize stable oxidation states of ceria-supported Pt_yO_x clusters in different environments. The collection of global minima for different stoichiometries resulting from the global optimisation effort is used to assess the effect of temperature, oxygen pressure, and support interactions on the phase diagrams, oxidation states, and structural properties of the Pt_yO_x particles. We thus identify favoured structural motifs and O/Pt ratios, revealing that oxidized states of ceria-supported particles are more stable than reduced ones under a wide range of conditions. These results indicate that studies rationalizing activity of ceria-supported Pt clusters must consider such oxidized states, and that previous understanding of such materials obtained only with fully reduced Pt clusters may be incomplete.

1. INTRODUCTION

Nanostructured materials based on ceria (CeO_2) and Pt have a wide range of applications in catalysis, such as in the three-way conversion in automobile exhausts,[1] in anode[2] or cathode[3] materials of fuel cells, or for mediating the water gas shift reaction,[4] among others.[5] CeO_2 is typically used in such materials as a non-inert support for the more active Pt phase, leading to intricate metal-support interactions that affect the electronic structure and chemical properties of both the metal and the oxide.[4,6–8] These electronic metal-support interactions further complicate the already challenging task of characterizing the properties of nanostructured catalytic materials, which are typically structurally complex. Their size, structure, and oxidation state not only depend on preparation conditions, but also often undergo significant transformations under reaction conditions, as revealed by *in situ* or *operando* spectroscopic techniques.[9–11] These structural and environmental complexities therefore hinder the straightforward computational modelling of working heterogeneous catalysts by means of first principles-based approaches.[12,13]

For systems based on Pt and ceria, Pt can be found in the form of nano- or subnano-particles of varying size,[4,7,14,15] or as single atoms either anchored to the ceria surface[2,16–18] or inserted in the ceria lattice.[19–21] Atomically dispersed Pt on ceria substrates has been studied extensively by means of combined experiment and computational approaches during the last decade because they allow to significantly increase specific activity for different reactions.[2,17,22] In such composites, Pt is often found in cationic form (i.e. Pt^{n+} species with n= 1, 2, or 4) either occupying Ce positions of the ceria lattice or deposited on undercoordinated sites of ceria substrates. The oxidation state of Pt atoms depends on their coordination environment and on the stoichiometry of ceria substrate, which can either accept or donate electrons by varying the occupation of the Ce4f states (reducing Ce^{4+} cations to Ce^{3+} and *vice versa*) and/or the amount of O in the ceria lattice.

Atomically dispersed Pt has often been distinguished from metallic nano- or subnano- Pt particles by the characteristic shifts of cationic Pt in X-Ray Photoemission Spectroscopy (XPS).[2,23,24] Nevertheless, recent studies report the formation of small oxidized Pt particles (i.e. PtO_x) under reaction conditions and suggest a relevant role of Pt-O-Pt motifs in activating oxidation reactions.[24–26] The interplay between stability, structure, and oxidation state of such ceria-supported PtO_x particles is however not well understood. In fact, during the last two decades, most studies modelling ceria-supported

Pt particles have considered non-oxidized states of Pt particles.[27–30] In addition, the majority of the aforementioned models (with notable exceptions)[25] were constructed by rather heuristic trial and error approaches, instead of using automated and unbiased global optimization or sampling approaches, which would ensure that the constructed models correspond to stable structures of the represented systems.

The use of sampling methods based on Monte Carlo approaches or of global optimization methods such as evolutionary algorithms have been available for years and applied quite successfully to determine the structure of supported metal or oxide clusters.[25,31–38] Of particular interest to characterizing the oxidation states of supported metal clusters are approaches that combine global optimization of various stoichiometries with a subsequent thermodynamic analysis,[35,36] or those that directly sample structure and stoichiometries under given conditions using grand canonical approaches.[25,32] The resulting phase-diagrams allow to pinpoint which states are stable under which conditions, relying on well-defined and stable structural models.

In order to identify the stable structures and oxidation states of ceria-supported Pt particles, we therefore combine a novel global optimization method with ab initio thermodynamics. We focus on the characterization of prevailing structural motifs, the effects of conditions on the stability of different oxidation states, and the role of the ceria support. In particular, we use a machine-learning assisted algorithm for the exploration of the configurational space.[39] Once the most stable structures have been determined for the targeted stoichiometries, their Gibbs Free energy of formation is evaluated under varying conditions by means of *ab Initio* thermodynamics (AITD).[40,41]

A consistent picture emerges for the formation and oxidation of both free-standing and ceria-supported PtO_x particles, revealing support-effects on the structural and compositional properties of PtO_x clusters, and the changes induced by exposure to different environmental conditions. Oxidized states of PtO_x clusters are found to be prevalent under a wide range of reaction conditions.

2. METHODS AND COMPUTATIONAL DETAILS

We carry out a systematic global optimization study based on Density Functional Theory (DFT) calculations and the "global optimization with first-principles energy expression (GOFEE)"[39] method in order to elucidate the stability of PtO_x oxidation states

under different conditions, the effects of particle size and a CeO_2(111) support, and the overall electronic structure of these systems.

We target Pt_yO_x clusters with y = 3 or 6 and x = 0 – 2y. Both free-standing and CeO_2(111)-supported structures are evaluated. For the CeO_2(111)-supported structures, only the supported particles are globally optimized, whereas the atoms of the CeO_2 surface are kept in their bulk-terminated positions. The structural characterization of each targeted stoichiometry consists on obtaining the configuration with the lowest internal energy, i.e. the Global Minimum (GM). Once the GM has been characterized for all the considered stoichiometries of the system, AITD is used to evaluate the free energies of each system and to generate the corresponding phase diagrams. In this section, we describe the global optimization strategy using GOFEE, the DFT calculations, and the AITD approach used.

2.1. GOFEE method and global optimization strategy

The GOFEE method allows to reduce the number of energy and force evaluations carried out at the DFT level by training, on-the-fly, a surrogate machine-learning energy model. This model is used to carry out local relaxations of every evaluated candidate and to guide the exploration of conformational space, which supposes a considerable improvement in computational efficiency with respect to other algorithms.[31,38] The GOFEE code therefore relies o a selected number of single point calculations at the DFT level, circumventing the need for carrying out more demanding local relaxations at costly levels of theory.

For each considered stoichiometry, the method follows the subsequent algorithm (illustrated in Figure 1):

1. An initial population of structures is generated randomly and its energy evaluated at the selected level of theory (DFT in our case, see below for more details).
2. The surrogate model is trained with these evaluated structures and their energies, and the structure population updated.
3. New candidates are generated.
4. The new candidates are locally relaxed using the surrogate model.

5. The most promising candidate according to an acquisition function is evaluated explicitly by DFT and added to the population.
6. The surrogate model is retrained with the updated population. Subsequent cycles start on step 3.

The number of cycles is strongly related to the quality of the putative global minimum structure found, up to a certain point where the algorithm converges (not always to the real global minimum) . Convergence is reached sooner for smaller systems, and we therefore allow a different of cycles for structures of different size:

- 200 cycles for free-standing Pt_3O_y stoichiometries.
- 300 cycles for free-standing Pt_6O_y stoichiometries.
- 400 cycles for supported Pt_3O_y stoichiometries.
- 800 cycles for supported Pt_6O_y stoichiometries.

For the generation of new candidates, the GOFEE method uses three different approaches. For the initial population it generates the candidates by placing the atoms randomly inside a box, checking that the atoms are not too close or too far from each other. For subsequent additions of candidates, two additional strategies are used as well, Permutation and Rattling, both transforming pre-existing structures. Permutation exchanges the positions of two atoms of different element selected at random and Rattling displaces one or more atoms in a structure by a random distance. The decision of which strategy is used to create a new candidate is stochastic. The probabilities of selecting each method are provided as a parameter and in the present work have been established as 0.6, 0.2, and 0.2 for random placement in a box, permutation and rattle Mutation generators, respectively. For the fully reduced systems, which do not globally optimize the positions of any O atom, Pt and O cannot be permuted and we chose 0.8 and 0.2 probabilities of random placement in a box and rattle mutation, respectively.

Due to the need to evaluate the energy of a large number of structures during the automated search for a global minimum, the DFT calculations during the GOFEE runs have been carried out using low-precision parameters and a simplified model of the $CeO_2(111)$ surface. The best structures for each stoichiometry have been subsequently recalculated at increasingly computationally demanding (and more precise) levels of theory (see next subsection for more details).

Our approach to optimize the structure of PtO_x particles uses five different levels of theory (i.e. combinations of parameters, functional, corrections, and structural models). The single-point calculations executed during each GOFEE run are carried out using low-level settings (see below for more details). All evaluated structures are subsequently filtered and relaxed at increasing levels of theory using low-level, mid-level and high-level local relaxations. These levels are briefly summarized Figure 2 and described in more detail in the following sections.

Before each set of local relaxations at an increased level of theory, structures are filtered to avoid duplicates by using the bag-of-bonds method.[31] This sorts the interatomic distances of a particle by length, and compares this list of distances between particles. Two particles are considered equal if δ_{max} and d_{max}, as defined in [31], are smaller than 0.3 and 0.7, respectively. Non-duplicate structures > 5 eV less stable than the obtained putative GM is also discarded. Due to the large number of structures and the limits of the bag-of-bonds approach when dealing with supported structures, in CeO_2-supported systems, an additional human-guided selection method is employed, where similar structures that have not been discarded by the bag-of-bonds method are excluded from subsequent relaxations. This approach allows saving considerable computational resources by filtering out unfit or duplicated structures at each level, only performing the increasingly costly optimizations on promising structures.

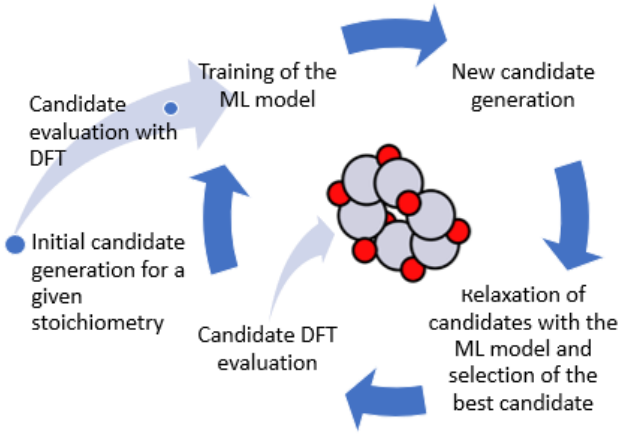

Figure 1: Representation of the algorithm followed by the GOFEE program.

2.1. Density functional theory calculations

The electronic structure of the considered systems have been determined by means of periodic calculations based on DFT. To this end, the Vienna Ab Initio Package

(VASP)[42,43] has been employed.

Free-standing particles were placed in a cubic cell of size 12 Å x 12 Å x 12 Å, which ensures negligible interactions between clusters in neighbouring cells while keeping calculations computationally affordable. For ceria-supported particles the oxide surface is represented by a 4x4 supercell of the CeO_2(111) surface, with 12 Å of vacuum surrounding the oxide slab. For all calculations the Brillouin zone is sampled using only the Γ point. In order to describe the interaction between the frozen core electrons and the valence electrons described explicitly by the electronic wave function, VASP uses the projector augmented wave method of Blöchl.[44]

All of the levels of theory share the aforementioned common characteristics of cell size and reciprocal space sampling. The low-, mid- and high- levels of theory use the Perdew-Wang (PW91) exchange-correlation functional[45] as it offers a good compromise between accuracy and computational cost.

Low-level settings consist on using a single O-Ce-O tri-layer to represent the ceria surface, which is kept fixed to the corresponding bulk positions. Spin-polarization is not allowed at this level, and the energy difference thresholds controlling the convergence of the self-consistent field are set to 10^{-4} eV for the energy cut-off of SCF iterations (EDIFF), the plane wave basis set energy cut-off is set for the minimum energy cut-off recommended in the PAW potentials for each atomic species (300 eV), and the PREC=Low flag of VASP.

The local optimization of selected structures at low-level settings only relaxes the Pt_yO_x particle, keeping the atoms from the ceria surface fixed, with a loose force convergence criterion of 0.1 eV/Å for the ionic relaxations.

The mid-level introduces the Hubbard +U correction. (i.e DFT+U, with U= 4eV), where a Coulomb-like interaction is applied only to the 4f valence orbitals of cerium, leading to the PW91+4 approach.[4,6,46–48] This partially corrects the inherent self-interaction error of semi-local density functionals, which otherwise leads to an incorrect delocalization of strongly correlated d and f electrons. The mid-level of theory also adds a second CeO_2 tri-layer to the surface slab model. The geometry of the upper CeO_2 tri-layer in contact with the platinum oxide is also allowed to relax, while the bottom tri-layer remains fixed. The converge parameters are the same as in the low-level relaxation.

The high-level approach adds spin polarization, increases the energy cut-off of the

plane wave basis set (400.0 eV) and increases the precision of the calculations setting the PREC=High in VASP. Although more computationally expensive, these calculations are performed over a small number of already optimized structures, and serve the purpose of obtaining accurate properties of the best surviving candidates.

A final relaxation of the most promising candidates has been performed using the HSE06 hybrid functional,[49–51] which includes a fraction of the exact Hartee-Fock exchange to overcome limitations of semi-local approximations to the exchange-correlation functional (instead of the Hubbard (+U) correction, which is no longer used).

Free-standing particles are optimized directly employing the high-level criteria, as the absence of a slab involves a drastically reduced computational cost. The final HSE06 relaxation is performed on all high-level optimized structures.

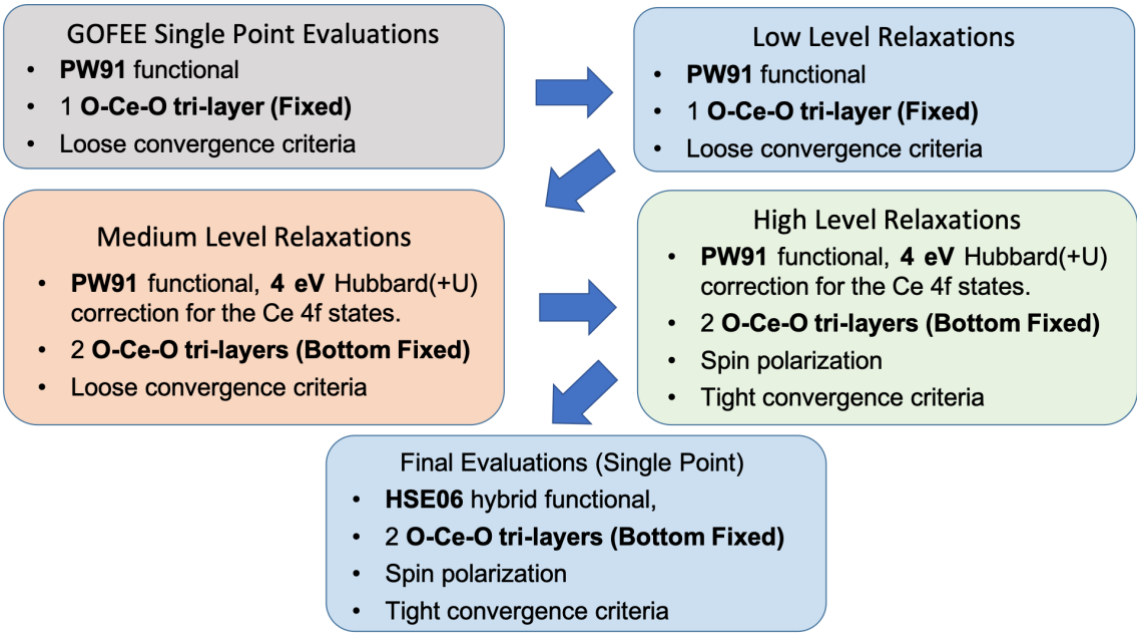

Figure 1. Schematic representation of the different levels of theory employed for the evaluation of the considered structures.

2.3. Ab Initio thermodynamics

Having obtained the putative GM for all of the considered stoichiometries, it is necessary to asses which of the compositions is most stable under different environmental conditions. Taking the formation energies using only the as-calculated absolute DFT energies is insufficient, since the stability of each oxidation state depends on how easy or

hard it is to obtain O atoms from the gas-phase environment in contact with these particles. We therefore carry out an ab initio thermodynamics (AITD) analysis, which allows to obtain Gibbs free energies of formation as a function of macroscopic properties of the system from energies obtained by ab initio methods at 0 K.

We calculate the Gibbs free energies of each state within the canonical ensemble. This assumes constant volume, temperature, and number of atoms of the system. We further assume the Pt_yO_x particles to be in equilibrium with a gas-phase reservoir of O_2 at a given T and p_{O2}. This means that their composition is going to be influenced by the T and p_{O2}. For any structure, the Gibbs free energy (G) is calculated as shown in equation 1:

$$G\left(Pt_yO_x/CeO_2\right) = U + TS + pV = U\left(Pt_yO_x/CeO_2\right) + F^{vib} + F^{conf} + pV \quad (1)$$

Where the internal energy (U) can be approximated as the total energy obtained in the DFT calculations of the system. F^{vib} and F^{conf} correspond to the vibrational and configurational contributions to the free energies, respectively. The Gibbs free energy of formation for the oxides is, thus, obtained by the difference of the Gibbs free energy of the oxide with the Gibbs free energy of the fully reduced cluster and the chemical potential of oxygen, related to temperature and pressure, as shown in equation 2.

$$\Delta G_f\left(Pt_yO_x/CeO_2\right) = G\left(Pt_yO_x/CeO_2\right) - G\left(Pt_y/CeO_2\right) - x\mu_O(T,P) \quad (2)$$

For the solid phase systems, the ΔF^{conf} and $\Delta(pV)$ terms are not significant at the pressures and temperatures typical of operando catalytic processes.[40,52] The F^{conf} and pV terms are similar for the different stoichiometries and cancel out when calculating relative (e.g. formation) free energies.

In turn, the vibrational contribution F^{vib} of small and supported metal-oxide clusters were found to depend on the low frequency contributions of the metal atoms only. The difference between clusters with the same number of metal atoms is therefore small. The differences in zero-point energy contributions are more significant, but proportional to the number of O atoms and accountable in an approximate way (~ 0.1 eV per O atom in the particle).[36]

The chemical potential of oxygen in the gas phase is evaluated in terms of the temperature and partial pressure of the molecular oxygen reservoir and the ZPE-corrected

DFT energy of molecular oxygen. Hence, for any value of the temperature, the chemical potential can be expressed as shown in equation 3:

$$\mu_O = \frac{E^{DFT}{}_{O_2} + \Delta\mu_{O2}(T, p_{O_2})}{2} = \frac{E^{DFT}{}_{O_2}}{2} + \Delta\mu_O(T, p_{O_2}) \quad (3)$$

With these approximations, the Gibbs free energy of formation for any Pt_yO_x, particle in any given chemical potential of oxygen is obtained as:

$$\Delta G_f(Pt_yO_x/CeO_2) = E^{DFT}(Pt_yO_x/CeO_2) - E^{DFT}(Pt_y/CeO_2) - x\left(\frac{E^{DFT}{}_{O_2} + E^{ZPE}{}_{O_2}}{2} + \Delta\mu_O(T, p_{O_2})\right) \quad (4)$$

For the free-standing particles, the same approximations are used, substituting the DFT energy of the ceria supported reduced particle by that of the free-standing particle. We use the same assumptions and approximations about the ΔF^{conf}, ΔF^{vib}, and $\Delta(pV)$ terms as for the ceria-supported particles, although these might not hold as well. Nonetheless, a complete vibrational analysis of the free-standing particles falls out of the scope of the present work.

A useful analysis tool obtained from this treatment are the phase diagrams where the most stable phase at different chemical potentials corresponds to the state with lowest ΔG_f.

3. Results and discussion

Structure, growth, and oxidation of the Pt_yO_x particles

We begin by describing the minimum energy structures found during the global minimum search for which the GOFEE method was employed. The considered Pt_yO_x stoichiometries are y=3 or 6 and x=0 - 2y for 20 different stoichiometries both free-standing and supported in a CeO_2(111) surface, which amounts to 40 systems differing in composition.

For each system a large number of structures were evaluated with DFT (up to 1613 for a single run of the most complex system – ceria supported Pt_6O_{12}) in order to locate the GM. Each stoichiometry is run at least twice, and if the minimum energy structures

of the runs don't coincide a third run of the algorithm is performed, which ensures that the obtained most stable structures are the best guess for each stoichiometry. After subsequent relaxations at increasing levels of theory, ~ 10 structures per stoichiometry are recalculated at the final HSE06 level.

The global minima obtained for the gas phase structures are depicted in Figure 3. For the fully or highly reduced structures, triangular Pt_3 motifs are prevalent and the structures are quite planar. As the particle becomes oxidized, it loses flatness in order to accommodate the new oxygen atoms while maintaining at least a mirror plane. This is prevalent for Pt_6O_x stoichiometries in low oxidation states but it loses importance for higher oxidation states. In higher oxidation states the size of the particle forces it to become either ringed or clustered, adopting one conformation or the other based on the platinum-to-oxygen ratio. Certain Pt:O ratios favor one structure or the other based on the possible formation of Pt-O bonds with certain structural characteristics.

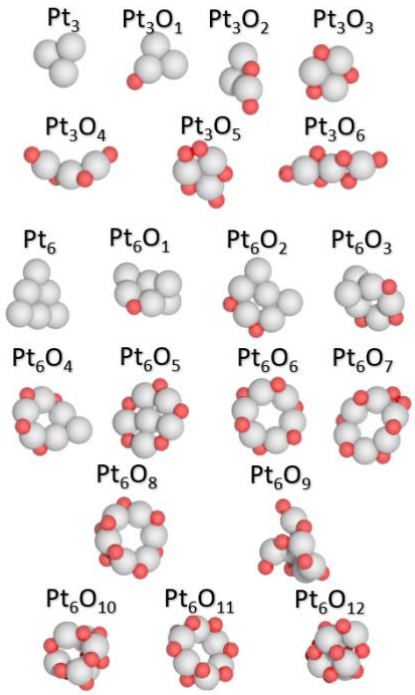

Figure 3. Most stable structures found for each stoichiometry of the free-standing systems. Red and grey spheres correspond to O and Pt atoms, respectively.

Oxygen atoms generally preferentially occupy bridge positions between Pt atoms. Additionally, some stoichiometries have global minima with oxygen atoms placed in terminal positions. PtO_x structures are therefore characterized by Pt-O-Pt angles between 80º and 100º, quasi-linear O-Pt-O angles, and Pt-O bond distances ~1.9 Å. Once every

bridge position between platinum pairs is filled, O atoms start to doubly occupy (opposite) bridge positions between two same Pt atoms, giving rise to the formation of planar PtO_4 motifs for highly oxidized states. Quasi-molecular forms of O pairs also appear in stable structures (see e.g. Pt_6O_7), although such motifs are less frequent.

For the ceria supported global minima (shown in Figure 4), the same structural motifs are present. However, the presence of the cerium oxide surface impedes the formation of strictly planar structures. Platinum atoms bind to oxygen atoms of the ceria surface and the oxygen atoms of the particle tend to locate near Ce. Since, distances between oxygen atoms in the ceria surface (~4.0 Å) are larger than the Pt-Pt bond distances (2.4 Å fully reduced, ~2.6 Å with an oxygen in bridged position), there is a size mismatch that causes the smaller particles to adopt triangular conformations where only two platinum atoms are in contact with the surface or angled conformations which allow a better fit.

For the Pt_3O_1-$CeO_2(111)$ and Pt_3O_5-$CeO_2(111)$ structures, a new motif appears where an oxygen is located between the three platinum atoms. This is favorable because it forms three linear O-Pt-O motifs with the oxygen positions in the surface, which confers enough stability to the particle to compensate the differences between the Pt-Pt bond length and the distance between surface oxygen atoms.

The inequivalence in surface oxygen distance and Pt-Pt bond length are less notable with the Pt_6O_x stoichiometries due to the increase in degrees of freedom, which allow the particle to adapt better to the surface. However, the tendency to form linear O-Pt-O bonds still proves to be significant since the observed minima include these motifs in all their structures, often bonding using O atoms from the ceria lattice to construct these linear motifs.

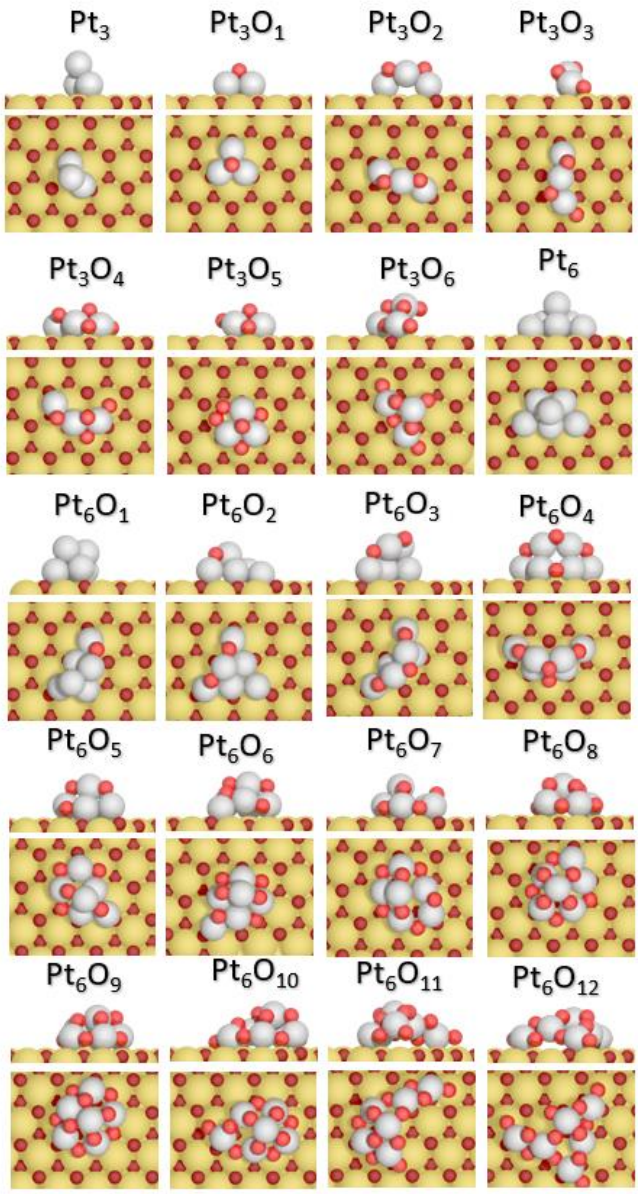

Figure 4. Most stable structures found for each stoichiometry of the CeO_2 (111) supported systems.

For low and medium oxidation states, the particles form more compact structures (e.g., $Pt_6O_9/CeO_2(111)$) where O atoms are shared between multiple platinum atoms. However, as particles become more saturated with oxygen atoms, they tend to spread over the surface, increasing the average coordination of Pt atoms while avoiding oversaturating individual platinum atoms.

Therefore, the two main differences between the conformations adopted by the $CeO_2(111)$ supported particles and the free-standing particles are due to the topology of the CeO_2 surface and to the possibility to form the aforementioned stable motifs with the

O atoms of the ceria surface.

Phase diagrams of the Pt_yO_x global minima

The variation for the free energy of the global minima found for each stoichiometry at different chemical potentials of the molecular oxygen reservoir is evaluated by means of AITD as described in the *methods and computational details* section. The Gibbs free energy of formation (ΔG_f) at each value of the chemical potential of the molecular oxygen reservoir (μ_O) for the global minimum of each stoichiometry is determined by equation 4. This allows the construction of phase diagrams where ΔG_f for each global stoichiometry is plotted in a range of μ_O, identifying the most stable stoichiometry for each value of the chemical potential and the values of μ_O at which phase transitions occur.

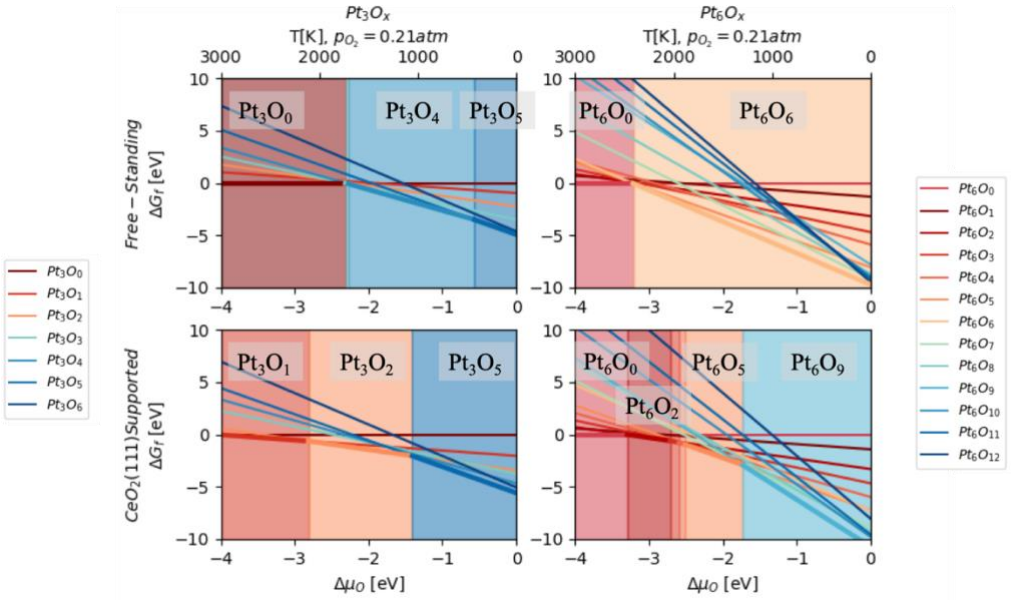

Figure 5. Phase diagrams for the free-standing (top) and $CeO_2(111)$-supported (bottom) Pt_yO_x systems calculated at the HSE06 level of theory.

The phase diagrams for the free-standing Pt_yO_x and $CeO_2(111)$-supported Pt_yO_x systems is shown in Figure 5, indicating the more stable stoichiometry for each value of μ_O.

Common to all systems, higher values of μ_O (corresponding to oxidizing environments) increase the stability of stoichiometries with a higher oxidation state, a direct consequence of the thermodynamic equilibrium with a molecular oxygen reservoir from which it is easier to extract O from (i.e. with a higher chemical potential to react).

Notably, partially oxidized states are stable for a wide range of μ_O, including very reducing conditions of down to $\Delta\mu_O \sim 3$ eV.

For the free-standing structures and the ceria-supported Pt_3Ox, the most stable structure at $\Delta\mu_O=0$ eV (T= 0K) is the structure with the Pt_3O_5 stoichiometry. For the free-standing Pt_6O_x system, Pt_6O_6 is the most stable configuration at $\Delta\mu_O=0$ eV, probably due to Pt:O ratio allowing it to forma a very stable ringed structure with the stable linear O-Pt-O and angled Pt-O-Pt motifs. For the ceria-supported Pt_6O_x systems the Pt_6O_9 structure made only of planar PtO_4 motifs is most stable under very oxidizing conditions (high $\Delta\mu_O$), indicating the stability of such structural motifs.

The evolution of the systems as $\Delta\mu_O$ decreases (e.g. temperature increases with fixed p_{O2}, as indicated in the upper x axis of Figure 5) is discussed next. Free-standing Pt_3O_5 is reduced at $\Delta\mu_O \sim -0.6$ eV to Pt_3O_4, and then to Pt_3O_0 at $\Delta\mu_O \sim -2.3$ eV. For the ceria-supported Pt_3O_x system, Pt_3O_5 is stable for a wider range of $\Delta\mu_O$ than its free-standing counterpart, becoming reduced to Pt_3O_2 at $\Delta\mu_O \sim -1.4$ eV, and later to Pt_3O_1 at $\Delta\mu_O \sim -3.8$ eV.

Free-standing Pt_6O_6 is stable for a wide range of $\Delta\mu_O$ and is reduced to Pt_6O_0 at only at $\Delta\mu_O \sim -3.2$ eV. Ceria-supported Pt_6O_9 is in turn reduced to Pt_6O_5 at $\Delta\mu_O \sim -1.8$ eV. In further reducing environments ($\Delta\mu_O \sim -1.8$ eV), the triangular Pt_6O_2 structure becomes the most stable conformation, and Pt_6O_0 is reached at $\Delta\mu_O \sim -3.3$ eV.

These results indicate that the ceria surface contributes to stabilizing more oxidized states of the PtO_x particles for some regions of the phase diagrams, but stabilizes more O-deficient states for others. A general stabilization of more O-deficient states would be expected due to the oxidizing behavior of the ceria surface, but our calculated phase diagrams demonstrate that intricate effects related to the kind of structures and structural motifs that each stoichiometry can form are more relevant than the oxidizing capacity of ceria.

Atomic charges of global minima

We now focus on the evolution of atomic charges in Pt atoms of the considered systems upon oxidation. The atomic charges (calculated by means of Bader's atoms in molecules approach)[53] of the Pt atoms of the most stable oxidation states of each system are shown on Figure 6. All considered stoichiometries follow similar trends in their charge distribution. As expected, as the system increases its oxidation states, so does the average

charge.

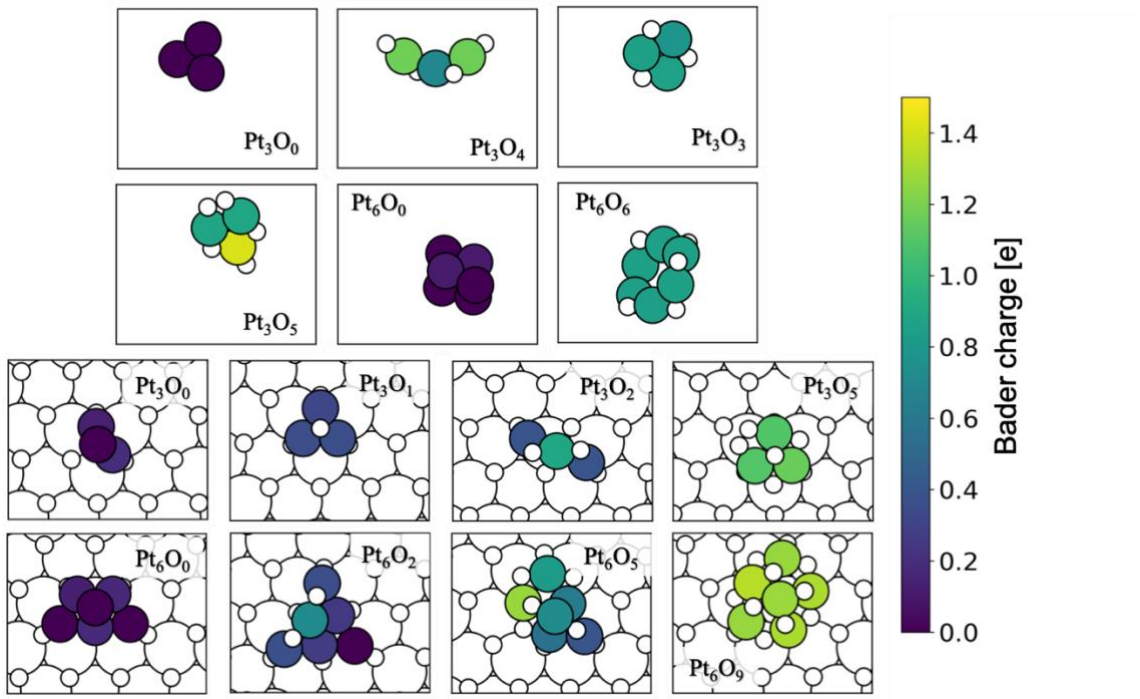

Figure 6. Charge distribution for the Pt atoms on each of the most stable oxidation states of the considered systems

Tied to this behavior is the distribution of charge. For platinum atoms coordinated to a single oxygen atom, the value of the charge is approximately 0.0-0.2 |e|. For Pt atoms bonded to two oxygen atoms, the charge increases to the 0.6-1.0 |e| range, while higher coordination numbers (i.e. Pt atoms in PtO_4 motifs) exhibit charges between 1.0-1.5 |e|. In systems where the Pt atoms are not equally coordinated, the differences in charge are more pronounced than in systems where all of the platinum atoms have a similar number of bonds to O. This indicates that the charge distribution is inhomogeneous. Furthermore, Pt atoms not bonded to oxygen atoms can have different charges depending on the charge of the Pt atoms they are coordinated to. For example, in the Pt_6O_2-CeO_2(111) stoichiometry the furthermost atom from the double Pt-O-Pt structure has a lower charge than the two neighboring ones, although this could also be due to the fact that this Pt atom has a larger Bader volume. The combination of these two effects helps explain the differences in charge in the free-standing Pt_3O_4 stoichiometry, where the central atom has a lower charge than the terminal ones as a consequence of sharing both of the oxygen atoms with other Pt atoms, while the terminal Pt atoms are bonded to a non-shared oxygen-atom.

It is also notable that the effect of the oxygen atoms in the ceria surface on the charge of the platinum atoms is slightly lower than that of the oxygen atoms adsorbed in the platinum cluster. This is visible when comparing the ceria-supported Pt_3O_5 structure to the free-standing counterpart. Despite the contact to atoms from the ceria surface, the Pt atoms of the Pt_3O_5 particle appear to be more oxidized for the free-standing case. Thus, although the $CeO_2(111)$ surface has an oxidizing effect on the particles and allows to complete certain stable structural motifs, bonds formed with O atoms from the ceria lattice are weaker and less oxidizing than those with O atoms directly on the PtO_x particles.

4. Conclusions

In this work, a systematic global optimization scheme has been employed in order to characterize free-standing and $CeO_2(111)$-supported Pt_yO_x structures, with y=3 and 6 and x=0-2y. The global optimization for each stoichiometry has been carried out with the GOFEE method, a novel approach which has proven to be fast and computationally efficient.

The morphological analysis of the obtained minima has revealed several structural motifs that are present in stable structures. Namely, the linear O-Pt-O, angled Pt-O-P (80-100º), square-planar PtO_4 formations, and the quasi-molecular O pairs. The $CeO_2(111)$ surface participates on the formation of such motifs, which leads to rather spread out structures for highly oxidized states.

The AITD analysis of the obtained global minima has revealed that oxidized particles are stable over a rather wide range of μ_O. Although the $CeO_2(111)$ surface has a slightly oxidizing effect, it generally does not stabilize states with lower oxidation states. This is related to the fact that O atoms from the $CeO_2(111)$ have a much weaker oxidizing effect than O atoms directly on the PtO_x clusters, as revealed by a detailed charge analysis.

In summary, the presented approach and resulting analysis constitutes a well-grounded and computationally efficient strategy for constructing representative structural models of the free-standing and $CeO_2(111)$ supported PtO_x clusters. This constitutes an improvement over non-machine-learning assisted global optimization algorithms or still prevalent human-guided approaches. It helps cement the combination of AITD with GO methods as a necessary step to characterize the structure and oxidation states of active sites preceding DFT-based mechanistic studies in catalysis.

The results of this work indicate that studies rationalizing activity of ceria-supported Pt clusters must consider oxidized states, and that previous understanding of such materials obtained only with fully reduced Pt clusters may be incomplete. Forthcoming studies comparing the chemical and catalytic properties of the different oxidation states will therefore be of pivotal importance. We expect these findings to be relevant also for other metal clusters on both inert and non-inert oxide supports such as ZnO and TiO_2.

5. Acknowledgements

Authors gratefully acknowledge support by the Spanish grants PGC2018-093863-B-C22 and MDM-2017-0767 as well as by the grants 2018BP00190 (for A.B.) and 2017SGR13 of the Generalitat de Catalunya. Computer resources have been provided by the Red Española de Supercomputación. This study was also supported the by European COST Action CA18234.

6. References

1. Crucq, A., Diwell, A. F., Rajaram, R. R., Shaw, H. A. & Truex, T. J. The Role of Ceria in Three-Way Catalysts. *Stud. Surf. Sci. Catal.* **71**, 139–152 (1991).

2. Bruix, A. *et al.* Maximum noble-metal efficiency in catalytic materials: atomically dispersed surface platinum. *Angew. Chem. Int. Ed. Engl.* **53**, 10525–10530 (2014).

3. Lim, D.-H., Lee, W.-D., Choi, D.-H. & Lee, H.-I. Effect of ceria nanoparticles into the Pt/C catalyst as cathode material on the electrocatalytic activity and durability for low-temperature fuel cell. *Appl. Catal. B Environ.* **94**, 85–96 (2010).

4. Bruix, A. *et al.* A New Type of Strong Metal−Support Interaction and the Production of H2 through the Transformation of Water on Pt/ CeO2(111) and Pt/CeOx/TiO2(110) Catalysts. *J. Am. Chem. Soc* **134**, 8968−8974 (2012).

5. Trovarelli, A. & Fornasiero, P. *Catalysis by ceria and related materials*. (Imperial College Press, London, UK, 2013).

6. Vayssilov, G. N. *et al.* Support nanostructure boosts oxygen transfer to catalytically active platinum nanoparticles. *Nat. Mater.* **10**, 310–315 (2011).

7. Lykhach, Y. *et al.* Counting electrons on supported nanoparticles. *Nat. Mater.* **15**, 284–288 (2016).

8. Lykhach, Y. *et al.* Oxide-based nanomaterials for fuel cell catalysis: The interplay between supported single Pt atoms and particles. *Catal. Sci. Technol.* **7**, 4315–4345 (2017).

9. Newton, M. A. Dynamic adsorbate/reaction induced structural change of supported metal nanoparticles: heterogeneous catalysis and beyond. *Chem. Soc. Rev.* **37**, 2644 (2008).

10. Kalz, K. F. *et al.* Future Challenges in Heterogeneous Catalysis: Understanding Catalysts under Dynamic Reaction Conditions. *ChemCatChem* **9**, 17–29 (2017).

11. Hansen, P. L. *et al.* Atom-resolved imaging of dynamic shape changes in supported copper nanocrystals. *Science* **295**, 2053–2055 (2002).

12. Bruix, A., Margraf, J. T., Andersen, M. & Reuter, K. First-principles-based multiscale modelling of heterogeneous catalysis. *Nat. Catal.* **2**, 659–670 (2019).

13. Grajciar, L. *et al.* Towards operando computational modeling in heterogeneous catalysis. *Chem. Soc. Rev.* **47**, 8307–8348 (2018).

14. Zhou, Y., Perket, J. M. & Zhou, J. Growth of Pt Nanoparticles on Reducible CeO_2(111) Thin Films : Effect of Nanostructures and Redox Properties of Ceria. *J. Phys. Chem. C* **2**, 11853–11860 (2010).

15. Shahed, S. M. F., Beniya, A., Hirata, H. & Watanabe, Y. Morphology of size-selected Pt n clusters on CeO 2 (111). *J. Chem. Phys.* **148**, 114702 (2018).

16. Pereira-Hernández, X. I. *et al.* Tuning Pt-CeO 2 interactions by high-temperature vapor-phase synthesis for improved reducibility of lattice oxygen. *Nat. Commun. 2019 101* **10**, 1358 (2019).

17. Nie, L. *et al.* Activation of surface lattice oxygen in single-atom Pt/CeO2for low-temperature CO oxidation. *Science* **358**, 1419–1423 (2017).

18. Dvořák, F. *et al.* Creating single-atom Pt-ceria catalysts by surface step decoration. *Nat. Commun.* **7**, 10801 (2016).

19. Tang, W. *et al.* Methane complete and partial oxidation catalyzed by Pt-doped CeO2. *J. Catal.* **273**, 125–137 (2010).

20. Bera, P. *et al.* Ionic Dispersion of Pt over CeO_2 by the Combustion Method: Structural Investigation by XRD, TEM, XPS, and EXAFS. *Chem. Mater.* **15**,

2049–2060 (2003).

21. Guo, H. *et al.* Synchrotron radiation photoelectron spectroscopy study of metal-oxide thin film catalysts: Pt–CeO_2 coated CNTs. *Appl. Surf. Sci.* **258**, 2161–2164 (2012).

22. Jones, J. *et al.* Thermally stable single-atom platinum-on-ceria catalysts via atom trapping. *Science* **353**, (2016).

23. Fiala, R. *et al.* High efficiency of Pt2+- CeO2novel thin film catalyst as anode for proton exchange membrane fuel cells. *Appl. Catal. B Environ.* **197**, 262–270 (2016).

24. Boronin, A. I. *et al.* CO oxidation activity of Pt/CeO_2 catalysts below 0 °C: platinum loading effects. *Appl. Catal. B Environ.* **286**, 119931 (2021).

25. Wang, H. *et al.* Surpassing the single-atom catalytic activity limit through paired Pt-O-Pt ensemble built from isolated Pt1 atoms. *Nat. Commun.* **10**, 3808 (2019).

26. Ke, J. *et al.* Strong Local Coordination Structure Effects on Subnanometer PtOx Clusters over CeO2 Nanowires Probed by Low-Temperature CO Oxidation. *ACS Catal.* **5**, 5164–5173 (2015).

27. Bruix, A. *et al.* A new type of strong metal-support interaction and the production of H_2 through the transformation of water on Pt/CeO_2(111) and Pt/CeO_x/TiO_2(110) catalysts. *J. Am. Chem. Soc.* **134**, 8968–8974 (2012).

28. Negreiros, F. R. & Fabris, S. Role of Cluster Morphology in the Dynamics and Reactivity of Subnanometer Pt Clusters Supported on Ceria Surfaces. *J. Phys. Chem. C* **118**, 21014–21020 (2014).

29. Ammal, S. C. & Heyden, A. Water-Gas Shift Activity of Atomically Dispersed Cationic Platinum versus Metallic Platinum Clusters on Titania Supports. *ACS Catal.* **7**, 301–309 (2017).

30. Aranifard, S., Ammal, S. C. & Heyden, A. Nature of Pt_n/CeO_2(111) Surface under Water–Gas Shift Reaction Conditions: A Constrained ab Initio Thermodynamics Study. *J. Phys. Chem. C* **116**, 9029–9042 (2012).

31. Vilhelmsen, L. B. & Hammer, B. A genetic algorithm for first principles global structure optimization of supported nano structures. *J. Chem. Phys.* **141**, 044711

(2014).

32. Liu, J. X., Su, Y., Filot, I. A. W. & Hensen, E. J. M. A Linear Scaling Relation for CO Oxidation on CeO2-Supported Pd. *J. Am. Chem. Soc.* **140**, 4580–4587 (2018).

33. Zhai, H. & Alexandrova, A. N. Fluxionality of Catalytic Clusters: When It Matters and How to Address It. *ACS Catal.* **7**, 1905–1911 (2017).

34. Zandkarimi, B. & Alexandrova, A. N. Dynamics of Subnanometer Pt Clusters Can Break the Scaling Relationships in Catalysis. *J. Phys. Chem. Lett.* **10**, 460–467 (2019).

35. Reichenbach, T. *et al.* Ab initio study of CO_2 hydrogenation mechanisms on inverse ZnO/Cu catalysts. *J. Catal.* **360**, 168–174 (2018).

36. Reichenbach, T., Walter, M., Moseler, M., Hammer, B. & Bruix, A. Effects of Gas-Phase Conditions and Particle Size on the Properties of Cu(111)-Supported ZnyOx Particles Revealed by Global Optimization and Ab Initio Thermodynamics. *J. Phys. Chem. C* **123**, 30903–30916 (2019).

37. Vilhelmsen, L. B. & Hammer, B. Identification of the Catalytic Site at the Interface Perimeter of Au Clusters on Rutile TiO 2 (110). *ACS Catal.* **4**, 1626–1631 (2014).

38. Vilhelmsen, L. B. & Hammer, B. Systematic Study of Au6 to Au12 Gold Clusters on MgO(100) F Centers Using Density-Functional Theory. *Phys. Rev. Lett.* **108**, 126101 (2012).

39. Bisbo, M. K. & Hammer, B. Efficient Global Structure Optimization with a Machine-Learned Surrogate Model. *Phys. Rev. Lett.* **124**, 86102 (2020).

40. Rogal, J. & Reuter, K. Ab Initio Atomistic Thermodynamics for Surfaces: A Primer. *Exp. Model. Simul. Gas- Surf. Interact. React. Flows Hypersonic Flights* 2–1 – 2–18 (2006).

41. Reuter, K. Ab Initio Thermodynamics and First-Principles Microkinetics for Surface Catalysis. *Catal. Letters* **146**, 541–563 (2016).

42. Kresse, G. & Furthmuller, J. Efficient iterative schemes for ab initio total-energy calculations using a plane-wave basis set. *Phys. Rev. B* **54**, 11169–11184 (1996).

43. Kresse, G. & Hafner, J. Ab initio molecular dynamics for liquid metals. *Phys. Rev. B* **47**, 558–561 (1993).

44. Blöchl, P. E. Projector augmented-wave method. *Phys. Rev. B* **50**, 17953–17979 (1994).

45. Perdew, J. P. *et al.* Atoms, molecules, solids, and surfaces: Applications of the generalized gradient approximation for exchange and correlation. *Phys. Rev. B* **46**, 6671–6687 (1992).

46. Bruix, A. *et al.* Maximum Noble-Metal Efficiency in Catalytic Materials: Atomically Dispersed Surface Platinum. *Angew. Chemie - Int. Ed.* **53**, 1–7 (2014).

47. Migani, A., Vayssilov, G. N., Bromley, S. T., Illas, F. & Neyman, K. M. Dramatic reduction of the oxygen vacancy formation energy in ceria particles: a possible key to their remarkable reactivity at the nanoscale. *J. Mater. Chem.* **20**, 10535 (2010).

48. Bruix, A. & Neyman, K. M. Modeling Ceria-Based Nanomaterials for Catalysis and Related Applications. *Catal. Letters* **146**, 2053–2080 (2016).

49. Heyd, J., Scuseria, G. E. & Ernzerhof, M. Hybrid functionals based on a screened Coulomb potential. *J. Chem. Phys.* **118**, 8207–8215 (2003).

50. Paier, J. *et al.* Screened hybrid density functionals applied to solids. *J. Chem. Phys.* **124**, 154709 (2006).

51. Ganduglia-Pirovano, M. V., Da Silva, J. L. F. & Sauer, J. Density-functional calculations of the structure of near-surface oxygen vacancies and electron localization on CeO_2(111). *Phys. Rev. Lett.* **102**, 026101 (2009).

52. Reuter, K. & Scheffler, M. First-Principles Atomistic Thermodynamics for Oxidation Catalysis: Surface Phase Diagrams and Catalytically Interesting Regions. *Phys. Rev. Lett.* **90**, 046103 (2003).

53. Bader, R. *Atoms in Molecules: A Quantum Theory*. (Oxford University Press, 1994).